

INFERRING DEPOLARIZATION OF CELLS FROM 3D-ELECTRODE MEASUREMENTS USING A BANK OF LINEAR STATE SPACE MODELS

Nour Zalmai, Reto A. Wildhaber, Désirée Clausen, and Hans-Andrea Loeliger

ETH Zurich

Dept. of Information Technology & Electrical Engineering
{zalmai, wildhaber, loeliger}@isi.ee.ethz.ch, desiree.clausen@alumni.ethz.ch

ABSTRACT

Cell depolarization runs essentially in a uniform motion along the muscular tissue, which creates transient electrical potential differences measurable by nearby electrodes. Inferring the depolarization speed and direction from measurements is of great interest for physicians. In cardiology, this is part of the inverse ECG problem which often requires a large number of electrodes and intense computational power even if the simple common model of the single equivalent moving dipole (SEMD) is applied. In this paper, we model a depolarization process as a straight-line movement of a SEMD. We provide an efficient algorithm based on linear state space models that infers the SEMD movement using only 3 measurement channels from a tetrahedral electrode and with the presence of interferences. Our algorithm is tested both on simulated and experimental data.

Index Terms— depolarization, linear state space models, electric dipole, tetrahedral electrode

1. INTRODUCTION

Depolarization of cells is a common phenomenon observed in biology for transmitting stimuli. While propagating information along neurons and contractile cells, such depolarization creates transient electrical potential differences measurable by nearby electrodes, as observed in the electrocardiogram (ECG) resulting from depolarization of heart muscle cells. Given those measurements we want to infer the speed and direction of the depolarization process. This knowledge can be exploited by physicians for medical diagnosis.

In the context of cardiology, this task is referred as the inverse ECG problem [1, 2] that aims to retrieve the myocardial polarization from electrode measurements. Usually a considerable number of surface electrodes and a prior anatomic geometry model collected by a magnetic resonance imaging (MRI) or computer tomography (CT) scan are presumed [3]. But still, the time-wise inversion of the electromagnetic equations is ill-posed. Therefore, different cardiac charge models with proper regularization [4] have been applied such as the simple and often used single equivalent moving dipole

(SEMD) model [5, 6] that reduces the cardiac charge distribution to a single electric dipole. Nonetheless inverting the SEMD equations [4] is still computationally intense.

To avoid heavy computations, we can exploit and track the SEMD trajectory. Thus, Bayesian filtering methods such as an Extended or Unscented Kalman filter can be envisaged as in [7, 8] where a magnetic dipole is tracked with magnetic field measurements. However, setting the parameters such as initial states and noise variances is burdensome. Furthermore, such methods are unable to detect whether a moving dipole is actually present or not. Similarly, sampling-based methods (e.g., sequential Monte Carlo techniques [9]) can be considered but in addition require substantial computational power.

In this paper, we use the SEMD model but our approach differs in two ways. First, we use a sensor equipped with a tetrahedral electrode resulting in 3 channels only. This tiny sensor profile opens opportunities for invasive (e.g., intracardiac) or semi-invasive (e.g., in the esophagus) measurements but outputs a low SNR due to small electrode distances. Secondly, we restrict the SEMD model to a uniform straight-line movement with constant dipole moment. Despite those constraints, we provide a robust and efficient algorithm for detecting and inferring the movement of a SEMD. In addition to its ability to run in real-time, the proposed algorithm copes with both a low SNR and the presence of interferences (e.g., caused by electrode motion artifacts).

After introducing the depolarization model and the multi-channel electrode in Section 2, this paper describes an algorithm inferring the speed and direction of the depolarization process. We model the voltage measurements with a bank of low-order linear state space models (LSSM) in Section 3. Efficient recursions to compute squared errors and a method for inferring the dipole movement even with the presence of interferences are provided in Section 4. In Section 5, we present the results on simulated and experimental data.

2. PHYSICAL MODEL OF CELL DEPOLARIZATION

We model a depolarization process as an electric dipole moving uniformly on a straight line while keeping the electric

dipole moment constant and aligned with the direction of movement. Using a coordinate system of an electrode with origin O , the position \mathbf{r}_k of the dipole at time index $k \in \mathbb{Z}$ is

$$\mathbf{r}_k = r\mathbf{d}_r + kv\mathbf{d}_v = r(\mathbf{d}_r + (k/\tau)\mathbf{d}_v), \quad (1)$$

where $r \in \mathbb{R}_+$ is the minimum distance to the origin O (achieved at $k = 0$, without loss of generality), $\mathbf{d}_r \in \mathbb{R}^3$ is the unit direction at this minimum distance, $v \in \mathbb{R}_+$ is the constant per-sample speed, $\mathbf{d}_v \in \mathbb{R}^3$ is the unit direction of movement, and $\tau = \frac{r}{v}$ is the time-scale parameter. It follows that $\langle \mathbf{d}_r, \mathbf{d}_v \rangle = 0$. The electric dipole moment $\mathbf{p} = p\mathbf{d}_p$ ($p \in \mathbb{R}_+$ and $\|\mathbf{d}_p\| = 1$) is such that $\mathbf{d}_p = \pm\mathbf{d}_v$.

Let \vec{M} denote an electrode point, $\beta = \|\vec{OM}\|$, and $\mathbf{d}_M = \vec{OM}/\|\vec{OM}\|$. The potential ϕ_k^M induced by the electric dipole at M and time index $k \in \mathbb{Z}$ is

$$\phi_k^M = \frac{1}{4\pi\epsilon} \frac{\langle \mathbf{p}, \beta\mathbf{d}_M - \mathbf{r}_k \rangle}{\|\beta\mathbf{d}_M - \mathbf{r}_k\|^3}, \quad (2)$$

where ϵ is the permittivity of the medium (assumed homogeneous). Let N be another electrode point at the same distance β to O . The quantity measured by the electrode M - N is $\phi_k^M - \phi_k^N$ and its 1st-order Taylor expansion in $\frac{\beta}{r}$ is

$$\begin{aligned} \phi_k^M - \phi_k^N &= \frac{p\beta}{4\pi\epsilon r^3} \frac{\langle \mathbf{d}_p, \mathbf{d}_v \rangle}{\left(1 + \left(\frac{k}{\tau}\right)^2\right)^{\frac{5}{2}}} \\ &\cdot \left\langle \mathbf{d}_M - \mathbf{d}_N, -\frac{3k}{\tau}\mathbf{d}_r + (1 - 2(k/\tau)^2)\mathbf{d}_v \right\rangle. \end{aligned} \quad (3)$$

Thus, the measured voltage is the projection of a 3D discrete-time signal into the electrode direction $\mathbf{d}_M - \mathbf{d}_N$. In order to infer the direction of depolarization in the 3D space, a multi-channel electrode is required with at least 4 points A, B, C , and D such that $(\mathbf{d}_A - \mathbf{d}_D, \mathbf{d}_B - \mathbf{d}_D, \mathbf{d}_C - \mathbf{d}_D)$ are linearly independent. For simplicity we choose ABC to form an equilateral triangle and D a summit such that $ABCD$ is a tetrahedron with $AD = BD = CD$ (cf. patent [10]). Denoting O the circumcenter of $ABCD$, the electrode points are at the same distance β to O . Combining the 3 measurement channels $\mathbf{V}_k = [\phi_k^A - \phi_k^D \quad \phi_k^B - \phi_k^D \quad \phi_k^C - \phi_k^D]^\top$, we get

$$\mathbf{V}_k = \lambda S^\top T F \mathbf{G}(k/\tau), \quad (4)$$

with

$$\mathbf{G}(t) = \frac{1}{(1+t^2)^{\frac{5}{2}}} \begin{bmatrix} t \\ 1 - 2t^2 \end{bmatrix} \quad (5)$$

$$S = [\mathbf{d}_A - \mathbf{d}_D \quad \mathbf{d}_B - \mathbf{d}_D \quad \mathbf{d}_C - \mathbf{d}_D] \in \mathbb{R}^{3 \times 3} \quad (6)$$

$$T = \langle \mathbf{d}_p, \mathbf{d}_v \rangle [\mathbf{d}_r \quad \mathbf{d}_v \quad \mathbf{d}_r \times \mathbf{d}_v] \in \mathcal{O}_3(\mathbb{R}) \quad (7)$$

$$F^\top = \begin{bmatrix} -3 & 0 & 0 \\ 0 & 1 & 0 \end{bmatrix}, \quad (8)$$

$\langle \mathbf{d}_p, \mathbf{d}_v \rangle = \pm 1$, and $\lambda = \frac{p\beta}{4\pi\epsilon r^3} \in \mathbb{R}_+$.

The matrix T contains the direction of the dipole movement and S accounts for the electrode geometry. Since the last row of F is all zero, $(\mathbf{V}_k)_{k \in \mathbb{Z}}$ is insensitive to a sign change of the last column of T . Thus, we should know a priori whether we track a depolarization (i.e., $\mathbf{d}_p = \mathbf{d}_v$) or a repolarization (i.e., $\mathbf{d}_p = -\mathbf{d}_v$). Alternatively, we could restrict the dipole movement to a half-space (e.g., \mathbf{d}_r such that $\langle \mathbf{d}_r, \mathbf{d}_A \rangle \geq 0$).

3. STATE SPACE MODEL

3.1. A LSSM for the Electrical Dipole Potentials

Similarly to [11], each component of $\mathbf{G}(t)$ is well approximated by a 2nd-order linear state space model

$$\hat{\mathbf{G}}(t) = \begin{bmatrix} K e^{-\frac{\omega_1}{r_1}|t|} \sin(\omega_1 t) \\ e^{-\frac{\omega_2}{r_2}|t|} \frac{\cos(\omega_2 |t| + \Phi_2)}{\cos \Phi_2} \end{bmatrix}, \quad (9)$$

with $r_1 = 0.64$, $\omega_1 = 1.139$, $K = 1.29$, $r_2 = 1.87$, $\omega_2 = 2.72$, and $\Phi_2 = 2.65$. Actually the 2nd component of $\mathbf{G}(t)$ is much better approximated with two 2nd-order LSSM but for conciseness we omit it. Using the following quantities

$$R(\omega) = \begin{bmatrix} \cos \omega & -\sin \omega \\ \sin \omega & \cos \omega \end{bmatrix} \quad (10)$$

$$A_E^p = \text{Diag} \left(e^{\frac{\omega_1}{\tau r_1}} R\left(\frac{\omega_1}{\tau}\right), e^{\frac{\omega_2}{\tau r_2}} R\left(\frac{\omega_2}{\tau}\right) \right) \in \mathbb{R}^{4 \times 4} \quad (11)$$

$$A_E^f = \text{Diag} \left(e^{-\frac{\omega_1}{\tau r_1}} R\left(\frac{\omega_1}{\tau}\right), e^{-\frac{\omega_2}{\tau r_2}} R\left(-\frac{\omega_2}{\tau}\right) \right) \in \mathbb{R}^{4 \times 4} \quad (12)$$

$$\mathbf{s}_E = [1 \quad 0 \quad 1 \quad 0]^\top \quad (13)$$

$$\tilde{C}_E = \begin{bmatrix} 0 & K & 0 & 0 \\ 0 & 0 & 1 & \tan \Phi_2 \end{bmatrix}, \quad (14)$$

we can generate $\hat{\mathbf{V}}_k$ with a 4th-order linear state space model

$$\hat{\mathbf{V}}_k = \begin{cases} \lambda S^\top T C_E (A_E^p)^k \mathbf{s}_E, & k \leq 0 \\ \lambda S^\top T C_E (A_E^f)^k \mathbf{s}_E, & k > 0 \end{cases}, \quad (15)$$

where $C_E = F \tilde{C}_E$. As the state transition matrices A_E^p and A_E^f depend on τ , we need one model per time scale.

3.2. A LSSM for the Interference Signals

In medical use, the electrodes often experience disturbances from external sources such as breathing or body movements, which create interferences. Since the dipole potentials may have a wide range of time scales and an overlapping frequency band with the interferences, selecting a pre-processing filter that does not distort the dipole signals is cumbersome.

Instead we locally model additive interferences with discrete-time polynomials of degree $n_I - 1$ that have a state space representation with transition matrix $A_I \in \mathbb{R}^{n_I \times n_I}$ having ones in the diagonal and upper-diagonal, an initial state $\mathbf{s}_I = [0 \quad \dots \quad 0 \quad 1]^\top \in \mathbb{R}^{n_I}$, and an observation vector depending on the coefficients of the polynomial. In agreement

with the LSSM of the dipole signals, we use one two-sided polynomial for each channel measurement and denote \tilde{C}_1^p , $\tilde{C}_1^f \in \mathbb{R}^{3 \times n_1}$ their observation matrices. Besides, at the meeting point of each two-sided polynomial we impose smoothness constraints such as continuity and differentiability of the counterpart continuous signals. Such linear constraints can be expressed as $[\tilde{C}_1^p \ \tilde{C}_1^f] = C_1 B_1$, with $B_1 \in \mathbb{R}^{d \times 2n_1}$ a fixed matrix whose row vectors span the subspace of constraints and $C_1 \in \mathbb{R}^{3 \times d}$ containing the coefficients to be estimated.

3.3. A Joint LSSM for the Measured Signals

What is measured by the electrode is thus the sum of the voltages induced by the moving electric dipole with some local polynomial interference. The two LSSM models can be stacked into a single one of order $n = 4 + n_1$ with $A_p = \text{Diag}(A_E^p, A_1)$, $A_f = \text{Diag}(A_E^f, A_1)$. $C_p = [\lambda S^T T C_E \ \tilde{C}_1^p]$, $C_f = [\lambda S^T T C_E \ \tilde{C}_1^f]$, $C = [C_p \ C_f]$, and $\mathbf{s} = [\mathbf{s}_E^T \ \mathbf{s}_1^T]^T$.

4. INFERRING DIPOLE MOVEMENTS

Assume we observe noisy measurements $\tilde{\mathbf{y}}_1, \dots, \tilde{\mathbf{y}}_K \in \mathbb{R}^3$ and want to detect a moving dipole at time step k , $k < K$.

4.1. Gaussian Noise Assumption and Localization

Due to the symmetry of the electrodes it seems reasonable to assume isotropic Gaussian measurement noise of variance σ^2

$$\tilde{\mathbf{y}}_k - C \mathbf{X}_k \stackrel{\text{iid}}{\sim} \mathcal{N}(0, \sigma^2 I), \quad (16)$$

where \mathbf{X}_k denotes the state vector of the LSSM. However, for simplifying the later optimization of the squared error we use the approximation $S^{-T} S^{-1} \approx \eta I$ such that

$$S^{-T} \tilde{\mathbf{y}}_k - S^{-T} C \mathbf{X}_k \approx \mathcal{N}(0, \tilde{\sigma}^2 I). \quad (17)$$

As our tetrahedral electrode has an equilateral triangle basis, SS^T is a diagonal matrix with two equal elements. Thus, by using such approximation $S^{-T} S^{-1} \approx \eta I$, η being the maximum eigenvalue of $S^{-T} S^{-1}$, we overestimate the noise in only one of the channel. In the particular case of a trirectangular tetrahedron, $(\overrightarrow{DA}, \overrightarrow{DB}, \overrightarrow{DC})$ forms an orthogonal basis and we exactly have $SS^T = \eta I$. We then define the squared-error between the pre-multiplied data $\mathbf{y}_k = S^{-T} \tilde{\mathbf{y}}_k$ and a similar model as before but with $C_p = [\lambda T C_E \ \tilde{C}_1^p]$ and $C_f = [\lambda T C_E \ \tilde{C}_1^f]$ (by abuse of notation).

In addition, for a real-time and stable implementation of our algorithm we localize the squared error with an exponential window of parameter $\gamma_\tau < 1$ (depending on τ only):

$$J_k(C, \tau) = \sum_{i=1}^k \gamma_\tau^{|i-k|} \|\mathbf{y}_i - C_p A_p^{i-k} \mathbf{s}\|^2 + \sum_{i=k+1}^K \gamma_\tau^{|i-k|} \|\mathbf{y}_i - C_f A_f^{i-k} \mathbf{s}\|^2. \quad (18)$$

Not only γ_τ localizes the cost with a forgetting effect of past dipole movements but also stabilizes the polynomial fit: the exponential decay counter-weights the polynomial growth.

4.2. Efficient Computation of the Cost Function

Both terms in (18) can be efficiently computed using forward/backward recursions [11]. The forward recursion is

$$\vec{W}_k = \gamma_\tau A_p^{-1} \vec{W}_{k-1} (A_p^{-1})^T + \mathbf{s} \mathbf{s}^T \quad (19)$$

$$\vec{\xi}_k = \gamma_\tau A_p^{-1} \vec{\xi}_{k-1} + \mathbf{s} \mathbf{y}_k^T \quad (20)$$

$$\vec{\kappa}_k = \gamma_\tau \vec{\kappa}_{k-1} + \|\mathbf{y}_k\|^2, \quad (21)$$

and the backward recursion is

$$\overleftarrow{W}_k = \gamma_\tau (A_f \overleftarrow{W}_{k+1} A_f^T + A_f \mathbf{s} \mathbf{s}^T A_f^T) \quad (22)$$

$$\overleftarrow{\xi}_k = \gamma_\tau (A_f \overleftarrow{\xi}_{k+1} + A_f \mathbf{s} \mathbf{y}_{k+1}^T) \quad (23)$$

$$\overleftarrow{\kappa}_k = \gamma_\tau (\overleftarrow{\kappa}_{k+1} + \|\mathbf{y}_{k+1}\|^2), \quad (24)$$

with $\vec{W}_0, \vec{\xi}_0, \vec{\kappa}_0, \overleftarrow{W}_K, \overleftarrow{\xi}_K$, and $\overleftarrow{\kappa}_K$ initialized with zeros.

Denoting $\kappa_k = \vec{\kappa}_k + \overleftarrow{\kappa}_k$ the cost function is

$$J_k(C, \tau) = \kappa_k - 2 \text{Tr} (C_p \vec{\xi}_k) + \text{Tr} (C_p \vec{W}_k C_p^T) - 2 \text{Tr} (C_f \overleftarrow{\xi}_k) + \text{Tr} (C_f \overleftarrow{W}_k C_f^T), \quad (25)$$

where $\text{Tr}(H) = \sum_i H_{i,i}$.

4.3. Minimizing the Cost Function

For a fixed time-scale τ , we focus on minimizing J_k . For conciseness we omit the time index k . We decompose $\vec{\xi} = \begin{bmatrix} \vec{\xi}_E \\ \vec{\xi}_1 \end{bmatrix}$, $\vec{W} = \begin{bmatrix} \vec{W}_E & \vec{W}_{E,1} \\ \vec{W}_{E,1}^T & \vec{W}_1 \end{bmatrix}$ such that $\vec{\xi}_E \in \mathbb{R}^{4 \times 3}$, $\vec{W}_E \in \mathbb{R}^{4 \times 4}$, $\vec{\xi}_1 \in \mathbb{R}^{n_1 \times 3}$, $\vec{W}_1 \in \mathbb{R}^{n_1 \times n_1}$, $\vec{W}_{E,1} \in \mathbb{R}^{4 \times n_1}$, and similarly, for the backward quantities. Denoting

$$\xi_E = C_E (\vec{\xi}_E + \overleftarrow{\xi}_E) \quad (26)$$

$$W_E = C_E (\vec{W}_E + \overleftarrow{W}_E) C_E^T \quad (27)$$

$$\xi_1 = B_1 \begin{bmatrix} \vec{\xi}_1 \\ \overleftarrow{\xi}_1 \end{bmatrix} \quad (28)$$

$$W_1 = B_1 \text{Diag}(\vec{W}_1, \overleftarrow{W}_1) B_1^T \quad (29)$$

$$W_{E,1} = C_E \begin{bmatrix} \vec{W}_{E,1} & \overleftarrow{W}_{E,1} \end{bmatrix} B_1^T, \quad (30)$$

the cost can be written as

$$J(\lambda, T, C_1) = \kappa - 2\lambda \text{Tr} (T \xi_E) + \lambda^2 \text{Tr} (W_E) - 2 \text{Tr} (C_1 \xi_1) + 2\lambda \text{Tr} (T W_{E,1} C_1^T) + \text{Tr} (C_1 W_1 C_1^T). \quad (31)$$

Minimizing this cost with respect to C_1 leads to

$$\hat{C}_1 = (\xi_1^T - \lambda T W_{E,1}) W_1^{-1} \quad (32)$$

$$\min_{C_1} J(\lambda, T, C_1) = \tilde{\kappa} - 2\lambda \text{Tr} (T \tilde{\xi}) + \lambda^2 \text{Tr} (\tilde{W}), \quad (33)$$

with $\tilde{\kappa} = \kappa - \text{Tr}(\xi_1^T W_1^{-1} \xi_1)$, $\tilde{\xi} = (\xi_E - W_{E,I} W_1^{-1} \xi_1)$, and $\tilde{W} = W_E - W_{E,I} W_1^{-1} W_{E,I}^T$. Then, since $\lambda \geq 0$, we have

$$\hat{T} = \underset{T \in \mathcal{O}_3(\mathbb{R})}{\text{argmax}} \text{Tr}(T \tilde{\xi}) = VU^T, \quad (34)$$

where $V, U \in \mathcal{O}_3(\mathbb{R})$ are from the SVD decomposition $\tilde{\xi} = U\Sigma V^T$ (cf. [12]). Denoting $(\hat{T})_i$ the i^{th} column of \hat{T} , for a depolarization, we have $\hat{\mathbf{d}}_r = (\hat{T})_1$, $\hat{\mathbf{d}}_v = \hat{\mathbf{d}}_p = (\hat{T})_2$ and for a repolarization, $\hat{\mathbf{d}}_r = -(\hat{T})_1$, $\hat{\mathbf{d}}_v = -\hat{\mathbf{d}}_p = -(\hat{T})_2$.

Finally we have $\hat{\lambda} = \text{Tr}(\Sigma) / \text{Tr}(\tilde{W})$ and

$$\min_{\lambda, T, C_1} J(\lambda, T, C_1) = \tilde{\kappa} - \frac{\|\tilde{\xi}\|_*^2}{\text{Tr}(\tilde{W})}, \quad (35)$$

with $\|H\|_*$ the nuclear norm (sum of singular values) of H .

4.4. Detection and Estimation

At time step k for a given time-scale τ , we test whether a moving dipole is present ($\lambda > 0$) or not ($\lambda = 0$) using the following log-likelihood ratio [13]

$$\text{LLR}_k^{(\tau)} = -\frac{1}{2} \ln \left(\frac{J_k(\hat{\lambda}, \hat{T}, \hat{C}_1, \tau)}{J_k(\lambda = 0, T = 0, \hat{C}_1, \tau)} \right) \quad (36)$$

$$= -\frac{1}{2} \ln \left(1 - \frac{\|\tilde{\xi}_k\|_*^2}{\tilde{\kappa}_k \text{Tr}(\tilde{W}_k)} \right), \quad (37)$$

where all quantities are defined in Subsection 4.3.

To encompass several time scales, τ is discretized: $\tau \in \{\tau_j, j \in J \subset \mathbb{N}\}$. Each τ_j has its own LSSM. Finally, if

$$\text{LLR}_k = \max_{j \in J} \text{LLR}_k^{(\tau_j)} \quad (38)$$

is above a threshold and locally maximum then a moving dipole is detected and the estimated dipole movement parameters can be retrieved using Subsection 4.3.

5. RESULTS

5.1. Performance on Simulated Data

We test our algorithm on simulated data generated using the dipole equation (2) with additive white Gaussian noise of variance $\sigma^2 = 10^{-4} \text{ V}^2$, a dipole with $\frac{p}{4\pi\epsilon} = 70 \text{ V} \cdot \text{m}^2$ and a tetrahedral electrode of sampling frequency 960 Hz. We use three different cases: 1) $r = 3 \text{ cm}$, $v = 4.1 \text{ m/s}$, 2) $r = 3 \text{ cm}$, $v = 5.8 \text{ m/s}$, 3) $r = 6 \text{ cm}$, $v = 5.8 \text{ m/s}$. For each case we vary the directions \mathbf{d}_r and \mathbf{d}_v to produce 7000 dipole movements. For the algorithm, τ is uniformly sampled from 3 to 16 with a step size of 1 and a polynomial of degree 2 is used to model interferences. The simulations are performed both without and with interference signals consisting of additive constants and cosines of different frequencies on each channel (respectively 4 Hz, 6 Hz, and 8 Hz).

As shown in Table 1, the algorithm demonstrates a good estimation ability even in the presence of these interference signals. Note that $(\mathbf{d}, \hat{\mathbf{d}})$ denotes the angle between the direction \mathbf{d} and the estimated direction $\hat{\mathbf{d}}$.

Errors	$\frac{ r-\hat{r} }{r}$ (%)	$(\mathbf{d}_r, \hat{\mathbf{d}}_r)$		$\frac{ v-\hat{v} }{v}$ (%)	$(\mathbf{d}_v, \hat{\mathbf{d}}_v)$			
Case 1	6.0	6.2	6.2°	7.7°	5.1	6.2	4.8°	6.0°
Case 2	5.1	5.8	6.6°	7.4°	5.1	5.9	5.3°	5.9°
Case 3	2.8	1.5	5.5°	16.4°	8.2	19.5	5.5°	14.7°

Table 1. Average errors for 7000 simulated dipole movements with (blue) and without (black) interferences.

5.2. Performance on Experimental Data

We also test our algorithm on experimental data. A sensor prototype including a tetrahedral electrode (cf. [10]) is placed inside a pot filled with saline water. The electric dipole consisting of two close-by electrodes charged with 2 V is attached to a string and pulled by a motor. Figure 1 shows a typical signal recorded while the dipole is moving and the estimated signals reconstructed with the LSSM from our algorithm. It is especially worth noticing the splitting of the approximated signal in dipole model and polynomial part.

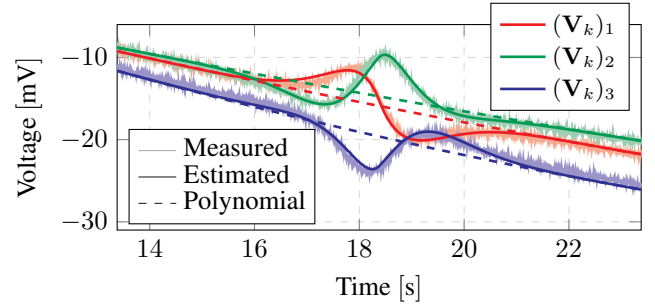


Fig. 1. Recorded signal, model fit and polynomial.

In Figure 2 we investigate the influence of an increase of the distance r . The black point represents the circumcenter of the electrodes and the green dashed lines the circle of radius with correct distance. The change of distance is accurately captured by our algorithm. The variations of \mathbf{d}_r are mainly caused by the experimental setup and not by the algorithm.

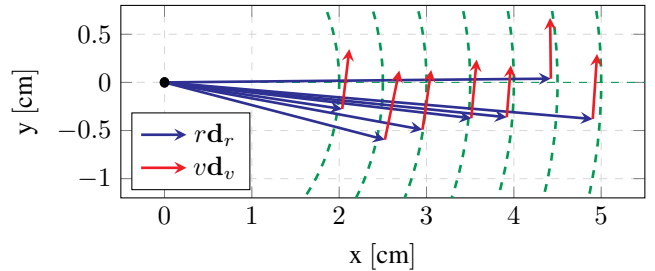


Fig. 2. Experiments with change of distance r

6. REFERENCES

- [1] J. J. M. Cuppen and A. Van Oosterom, "Model studies with the inversely calculated Isochrones of ventricular depolarization," *IEEE Transactions on Biomedical Engineering*, no. 10, pp. 652–659, 1984.
- [2] R. M. Gulrajani, "The forward and inverse problems of electrocardiography," *IEEE Engineering in Medicine and Biology Magazine*, vol. 17, no. 5, pp. 84–101, 1998.
- [3] K. Sohn, L. Wener, L. Kichang, A. M. Galea, G. B. Hirschman, A. M. Hayward, R. J. Cohen, and A. A. Armoundas, "The single equivalent moving dipole model does not require spatial anatomical information to determine cardiac sources of activation," *IEEE Journal of Biomedical and Health Informatics*, vol. 18, no. 1, pp. 222–230, 2014.
- [4] S. Guofa, J. Mingfeng, X. Ling, W. Qing, L. Feng, and S. Crozier, "A comparison of different choices for the regularization parameter in inverse electrocardiography models," in *IEEE International Conference on Engineering in Medicine and Biology Society (EMBS)*, 2006, pp. 3903–3906.
- [5] Y. Fukuoka, T. F. Oostendorp, D. A. Sherman, and A. A. Armoundas, "Applicability of the single equivalent moving dipole model in an infinite homogeneous medium to identify cardiac electrical sources: A computer simulation study in a realistic anatomic geometry torso model," *IEEE Transactions on Biomedical Engineering*, vol. 53, no. 12, pp. 2436–2444, 2006.
- [6] R. M. Gulrajani, F. A. Roberge, and P. Savard, "Moving dipole inverse ECG and EEG solutions," *IEEE Transactions on Biomedical Engineering*, vol. BME-31, no. 12, pp. 903–910, 1984.
- [7] M. Birsan, "Unscented particle filter for tracking a magnetic dipole target," in *OCEANS MTS/IEEE Proceedings*, 2005, pp. 1656–1659.
- [8] N. Wahlstrom, J. Callmer, and F. Gustafsson, "Single target tracking using vector magnetometers," in *IEEE International Conference on Acoustics, Speech and Signal Processing (ICASSP)*, 2011, pp. 4332–4335.
- [9] H. R. Mohseni, E. L. Wilding, and S. Sanei, "Sequential Monte Carlo techniques for EEG dipole placing and tracking," in *Sensor Array and Multichannel Signal Processing Workshop*. IEEE, 2008, pp. 95–98.
- [10] R. A. Wildhaber, "System and method for providing a representation of cardiac cell charge state," 7 2015, Patent CF/00961/15.
- [11] N. Zalmi, C. Kaeslin, L. Bruderer, S. Neff, and H.-A. Loeliger, "Gesture recognition from magnetic field measurements using a bank of linear state space models and local likelihood filtering," in *IEEE International Conference on Acoustics, Speech and Signal Processing (ICASSP)*, 2015.
- [12] P. H. Schönemann, "A generalized solution of the orthogonal procrustes problem," *Psychometrika*, vol. 31, no. 1, pp. 1–10, 1966.
- [13] L. Bruderer, H.-A. Loeliger, and N. Zalmi, "Local statistical models from deterministic state space models, likelihood filtering, and local typicality," in *IEEE International Symposium on Information Theory (ISIT)*, 2014, pp. 1106–1110.